

One Step Photocatalytic Selective Oxidation of p-Methoxy Toluene over TiO₂/Graphene Composite in Comparison of Pure TiO₂

Haitham El-Bery, Yoshihisa Matsushita, Ahmed Abdel-moneim

Egypt-Japan University of Science and Technology, Department of Materials Science and Engineering
P.O. Box 179, New Borg El-Arab City Postal Code 21934, Alexandria, Egypt

Haitham.Mohamed@Ejust.edu.eg; Matsushita.Yoshihisa@ejust.edu.eg;

ahmed.abdelmoneim@ejust.edu.eg

Abstract -Photocatalytic production of p-anisaldehyde in one step reaction over TiO₂/graphene and pure TiO₂ p25 was investigated. The photocatalytic reaction was performed using molecular oxygen (O₂ flow rate =2.91 ml/min) as oxidant and UV-LED light irradiation source (I=224 mW/cm²) as the driving force in a rectangular quartz cell as batch reactor. The hydrothermal method was used to synthesize TiO₂/graphene composite. X-ray diffraction (XRD), UV-Visible spectrophotometer, Fourier-transform infrared spectroscopy (FTIR), scanning electron microscopy (SEM), nitrogen adsorption desorption isotherm and the Brunauer-Emmett-Teller (BET) surface area tests were employed to determine the structural features and properties of the photocatalysts. It is found that TiO₂/G improves both the yield and selectivity (76 and 65 %) in comparison to the pure TiO₂ (69 and 57 %), while the conversion efficiency didn't show a significant change. Moreover, it is revealed from the results that the rate of the oxidation reaction increased by 50 % in case of TiO₂/G composite in comparison of pure TiO₂ p25.

Keywords: Photocatalysis – Selective oxidation- p-anisaldehyde- TiO₂/G composite

1. Introduction

The selective oxidation of alcohols into carbonyl compounds using molecular oxygen instead of conventional toxic or corrosive stoichiometric oxidants such as Cl₂, ClO⁻, Cr (IV), is one of the most challenging functional groups transformations (Mallat & Baiker, 2004; M. Zhang et al., 2009) and of a great industrial importance. This is due to the fact that carbonyl groups such as aldehydes and ketone derivatives are widely utilized in fragrance, confectionary and pharmaceutical industries (Palmisano et al., 2010; Palmisano, Augugliaro, Pagliaro, & Palmisano, 2007).

In order to overcome the disadvantages of the conventional organic synthesis of carbonyl groups many researchers focused on exploiting environmentally clean processes for organic synthesis of carbonyl groups from corresponding alcohols. The oxidation of alcohols using molecular oxygen has been successfully realized by using noble metals and transition metals catalysts (Mueller, Goller, & Sigman, 2004; Palmisano et al., 2007).

Moreover, photocatalysis using active oxide semiconductors has attracted a lot of attention since the breakthrough done by Fujishima and Honda in 1972. This is mainly due to its high oxidation potential, environmentally friendly features and the benefit of using molecular oxygen as oxidant and light as the driving force which is a potential and promising strategy for this purpose (Yang, Zhang, & Xu, 2013; N. Zhang et al., 2011). These photocatalysts absorb light that have photon energy (hu) matching or exceeding the band gap energy (E_g) of the semiconductor. This causes an electron in the VB is excited into the CB, leaving a positive hole in the VB. These photogenerated holes and electrons play a very important role in hydrogen production, pollutant degradation, photocatalytic disinfection, and solar energy conversion. However, the photogenerated electrons and holes in the excited states are unstable and can easily recombine dissipating the input energy as heat, which result in low efficiency of

photocatalysis (Hoffmann et al., 1995; Kudo & Miseki, 2009). During the past decade, a variety of strategies have been employed so as to improve the photocatalytic performance of semiconductor photocatalysis by doping, noble metal loading, improving the morphological designs and utilizing semiconductor composites (Ksibi, Rossignol, Tatibouët, & Trapalis, 2008; Lee, Park, & Joo, 2006). Other attempts have been conducted to combine graphene with semiconductor photocatalysts to enhance their photocatalytic activity by acting as electric shuttle and mechanical support (Pan et al., 2012). This due to graphene exceptional properties such as excellent electron mobility at room temperature ($200\,000\text{ cm}^2\text{ V}^{-1}\text{ s}^{-1}$), large theoretical surface area of $2600\text{ m}^2/\text{g}$, high thermal conductivity of 5000 W/m K , and optical transparency (Geim, Novoselov, Geim A. K., & Novoselov K. S., 2007; Geim, 2009). In comparison with pure TiO_2 , the enhanced photocatalytic effect of graphene- TiO_2 composite was generally attributed to three factors: including electron-hole pair separation by electron injection into graphene that can act as electron sink hindering recombination while the hole remains in TiO_2 to drive the oxidation reaction, increasing the light absorption, and increasing the reaction possibility by boosting reactant adsorbability (Pan et al., 2012).

In this investigation we exploit the benefits of synergistic photocatalytic effect of the TiO_2 /graphene composite in comparison to pure TiO_2 in one step photocatalytic oxidation reaction starting by p-methoxy toluene to produce p-anisaldehyde in batch reactor with high yield and selectivity.

2. Experimental Section

2. 1. Preparations: Graphene Oxide

Graphene oxide was prepared via modified Hummer method (Marcano et al., 2010). Briefly, a 9:1 mixture of concentrated $\text{H}_2\text{SO}_4/\text{H}_3\text{PO}_4$ (360:40 mL) was added to a mixture of graphite powder (3.0 g, 1 wt equiv) and KMnO_4 (18.0 g, 6 wt equiv), the reaction is slightly exothermic causing a rise in temperature to $35\text{--}40\text{ }^\circ\text{C}$. The reaction was then heated to $50\text{ }^\circ\text{C}$ and stirred for 12 h. The reaction was cooled to rt and poured onto ice (400 mL) with 30% H_2O_2 (3 mL), the solid material was then washed in succession with 200 mL of water, 200 mL of 30% HCl, and 200 mL of ethanol (2). The solid obtained was vacuum-dried overnight at $50\text{ }^\circ\text{C}$.

2. 2. TiO_2 /Graphene Composite

The hydrothermal method was used for the synthesis of the TiO_2 /graphene composite. 50 mg GO was put into a solution of 60 mL deionized water and 40 mL ethanol under sonication for 1 h to re-exfoliate the GO thoroughly, meanwhile 0.95 g TiO_2 p25 was dispersed in 20 mL deionized water for 30 min, which then was added to the GO solution dropwise under stirring for 2h until a homogenous suspension was obtained. The suspension was then poured into Teflon-lined autoclave (160 mL) and maintained at $200\text{ }^\circ\text{C}$ for 12 hrs to finally synthesis TiO_2 /G composite which was filtered and washed with deionized water several times and dried at ambient conditions.

2. 3. Characterization

The morphology of the photocatalysts was characterized by scanning electron microscope (SEM- JEOL-JSM-6010LV). The X- ray diffractometer (Lab XRD-6100 Shimadzu, Japan) equipped with $\text{Cu K}\alpha$ radiation source with wavelength ($\lambda= 1.5418\text{ \AA}$) was used to characterize the crystallinity and the phase structure of the prepared samples. The FTIR measurements were performed on (Vertex 70, Bruker scientific instruments, Germany) IR spectrometer while the UV-Visible spectrophotometer was used to measure the samples absorbance. Nitrogen adsorption-desorption isotherms and the Brunauer-Emmett-Teller (BET) surface areas were collected at 77 K using (BelsorbminiII, BEI Japan inc., Japan).

2. 4. Experimental Setup

The photocatalytic reaction was performed in a quartz rectangular cell (1 x 1 x 4.5 cm) W, L and H respectively, with a 9.5 cm neck tube opening, which was used as batch reactor with 4 mL total volume.

It was placed 1 cm from the UV-LED, which assures efficient penetration of UV light through the whole reactor volume due to UV transparency of quartz and cell small dimensions.

In all the experiments, 1 wt% of p-MT suspension in ethyl acetate (4 ml) was used, in which 2.5 g/L of TiO₂/G powder was added. The reactant mixture was first stirred in the batch cell at 800 rpm by using a magnetic stirrer for 1 hour in the dark for adsorption-desorption equilibrium. Then, oxygen gas was continuously fed from oxygen reservoir into the mixture through 1/16" polymeric tubing at the adjusted flow rate (2.91 ml/min) by using a micro-plunger pump (CP-DSM-GF, VICI Valco-Instruments, USA). After that, the cell was UV-irradiated for 4 hrs at ambient temperature and pressure using a UV-LED lamp with the peak emission of 365 nm from which the light intensity was in the range of (224 mW/cm²) (NLBU21P02, Nichia Corporation, Japan).

For identification of the reactant and products concentrations, samples were withdrawn from the reaction mixture at stipulated time intervals and were analyzed by GC-MS (GCMS-QPultra2010, Shimadzu, Japan). Conversion of p-methoxy toluene (p-MT), yield of aldehyde, and selectivity for aldehyde were defined as follows:

$$\text{Conversion (\%)} = [(C_0 - C_{p\text{-MT}}) / C_0] \times 100$$

$$\text{Yield (\%)} = C_{\text{aldehyde}} / C_0 \times 100$$

$$\text{Selectivity} = [C_{\text{aldehyde}} / (C_0 - C_{p\text{-MT}})] \times 100$$

Where C₀ is the initial concentration of the p-MT however, C_{p-MT} and C_{aldehyde} are the concentration of the reactant and the corresponding aldehyde, respectively, after certain time.

3. Results and Discussion

3. 1. Structural And Chemical Characterization:

Fig.1 (a and b) shows the structural morphology of the TiO₂ p25 and TiO₂/graphene composite respectively. It can be noticed that TiO₂ p25 NPs form dense agglomerates on the reduced graphene oxide nano-sheets (b) which can be related to the tendency of TiO₂ NPs to be easily anchored on RGO to form Ti-O-C bond with RGO at location of defects, after that NPs prefer to form agglomerates around these spots.

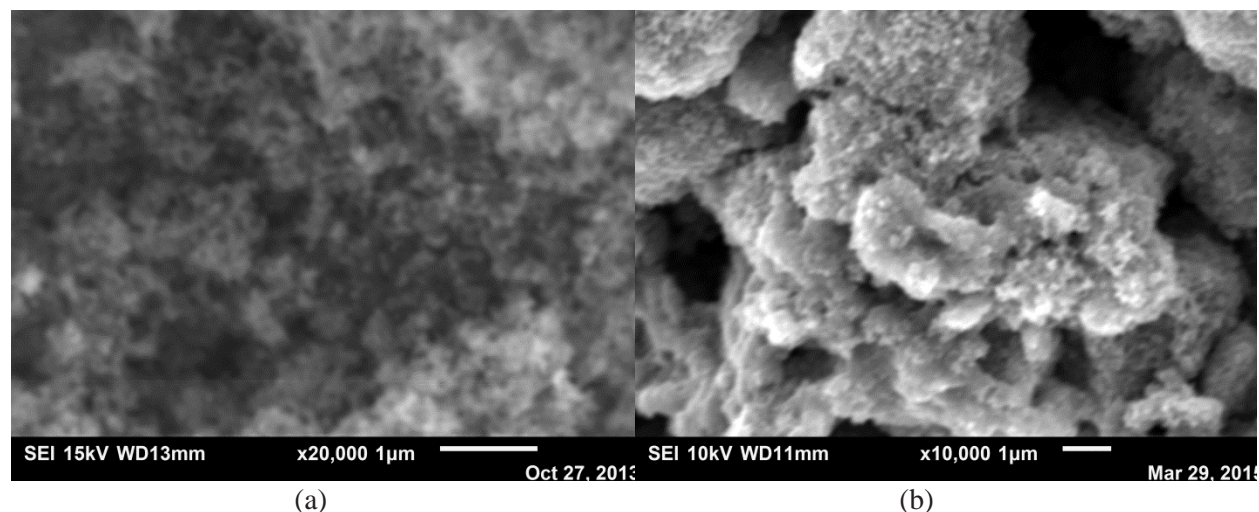


Fig.1. SEM images of (a) TiO₂ p25 nanoparticles and (b) TiO₂/ graphene composite.

X-ray diffraction pattern (XRD) was used to determine the crystalline phase of the prepared photocatalysts as shown in Fig.2. TiO₂/graphene (Red line) showed a similar pattern like pure TiO₂ p25 (black line) which can be attributed to the low weight ratios of RGO in the prepared composite along with weak intensity of graphene, in addition the main characteristic peak of RGO at 25.0 which most probably shadowed by the (101) peak at 25.3° of anatase TiO₂ which is similar to previous reports. Pure TiO₂ p25 with typical diffraction peak (101) anatase phase along with other peaks (103), (004), (112), (200), (105), etc. and a rutile peak (110) along with a relatively weak peaks of (101), (111), (211), and (220)

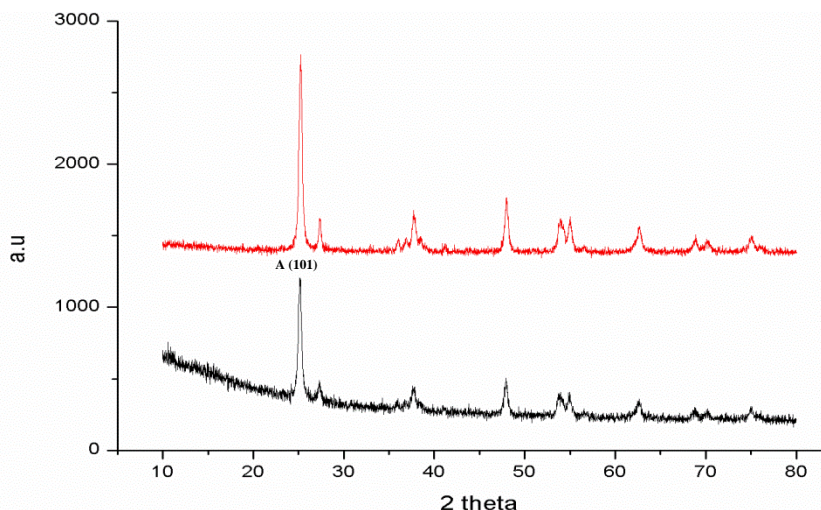


Fig. 2. X-ray diffraction pattern (XRD) of TiO₂ p25 (black) nanoparticles and TiO₂/graphene composite (red)

Fig.3 (A) shows the UV-Visible spectrophotometer of the samples which indicates a little shift in absorption towards the visible region in case of TiO₂/G in comparison to pure TiO₂. Moreover, The (FTIR) transmission spectra of TiO₂ p25 NPs and TiO₂/G were shown in Fig.3 (B). Both samples show low frequency bands around 650 cm⁻¹ which were attributed to the vibration of Ti-O-Ti. The spectra broadening below 1000 cm⁻¹ in case of TiO₂/G compared to pure TiO₂ can be attributed to the formation of Ti-O-C bond during the hydrothermal process overlapping with original peak of Ti-O-Ti vibration. Moreover the observed peak at 1600 cm⁻¹ for TiO₂/G indicates the skeletal vibration of reduced grapheme oxide. In addition the broad absorption from 3000-3700 cm⁻¹ was caused by the O-H stretching vibration of the surface physically adsorbed water.

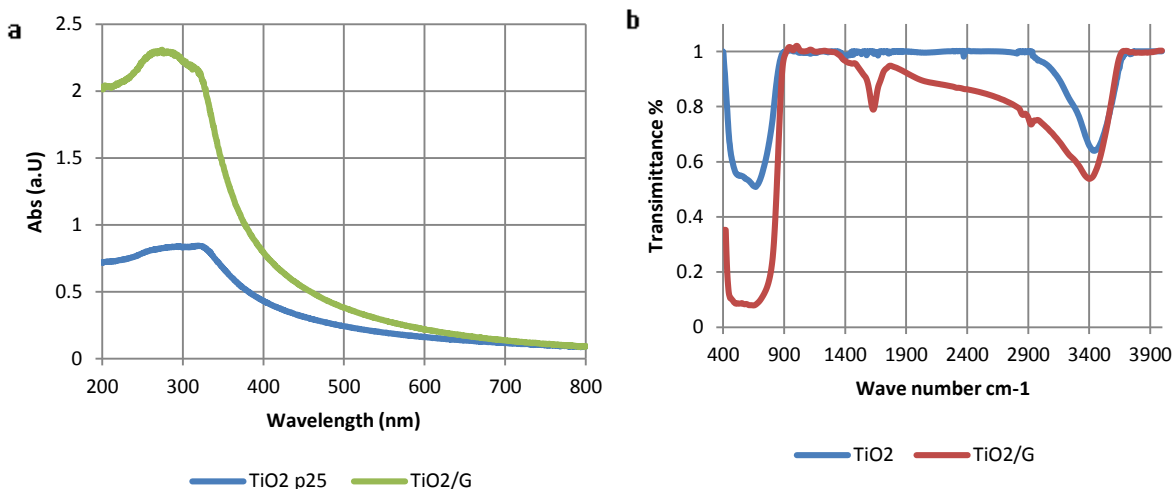


Fig.3. UV-Visible spectrophotometer (A) and Fourier transform infrared spectra of TiO₂ p25 nanoparticles and TiO₂/graphene composite

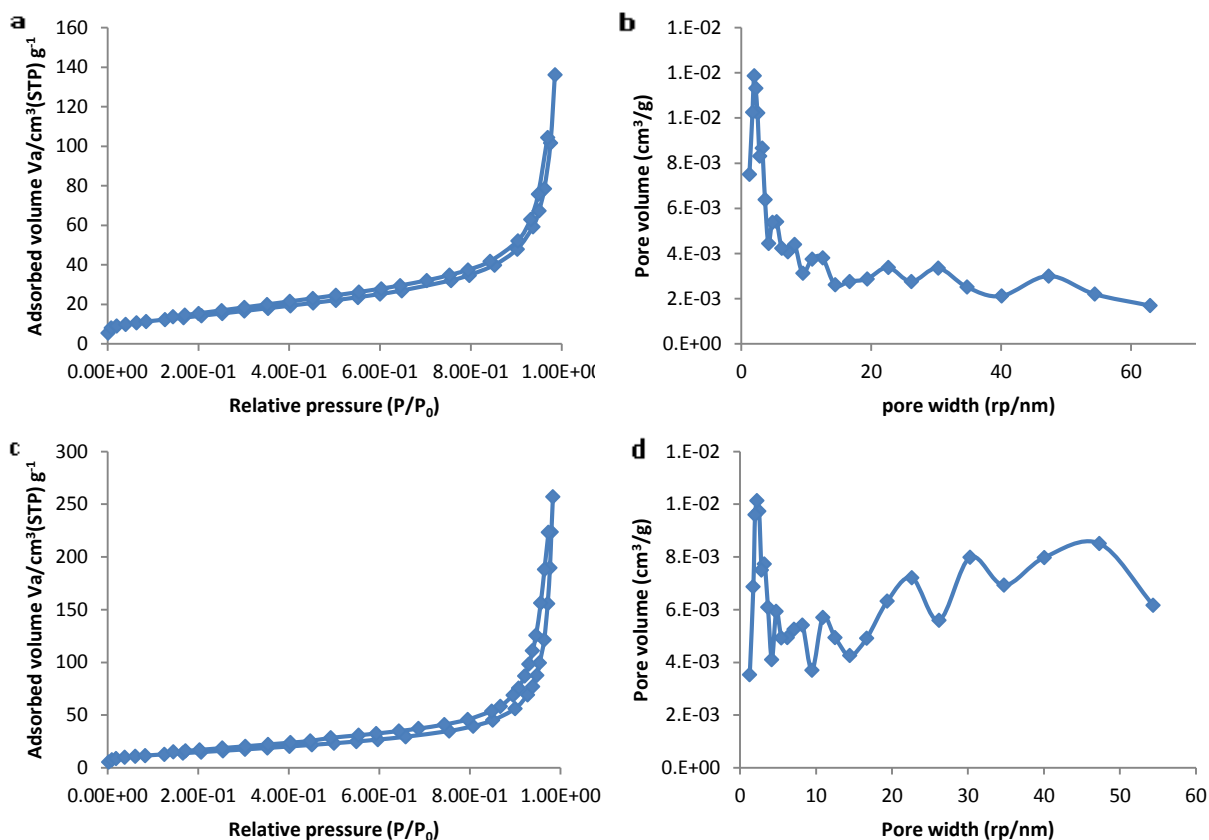


Fig.4. BET adsorption-desorption isotherm and pore size distribution of TiO_2 p25 nanoparticles (a and b) and $\text{TiO}_2/\text{graphene}$ composite (c and d)

In order to explore the effect of graphene on the porosity and surface area of the prepared composite, and thus understand its effect on the photocatalytic performance, we measured BET surface areas, surface porosity and N_2 adsorption-desorption isotherm as shown in Fig.4. According to IUPAC classification (Kenneth et. al., 1985), it can be seen that both samples shows type IV isotherm with a typical H3 hysteresis loop characteristic to mesoporous solids which confirmed by the pore size distribution shown in Fig.4.

3. 2. Photocatalytic Study

Fig. 5 shows the online analysis of the concentrations of p-methoxy toluene (reactant), p-methoxy benzaldehyde and p-methoxy toluene (products) versus the irradiation time for both catalysts (a, and c) which indicate that p-methoxy toluene concentration decreases with time, while, p-methoxy benzaldehyde concentration increases until it reaches a peak then start to decrease due to further oxidation to the corresponding acid (p-methoxy benzoic acid) which can be further degraded to CO_2 . In addition Fig. 5 (b, and d) shows the conversion efficiency, yield and selectivity percents, in which TiO_2/G composite gives higher yield and selectivity but a comparable conversion as compared with pure TiO_2 as further indicated at Table 1. Moreover, it is found that the oxidation reaction kinetics follow the pseudo-first order reaction in which the rate constant in case of TiO_2/G composite (0.21 min^{-1}) was nearly double the rate in case of pure TiO_2 (0.14 min^{-1}).

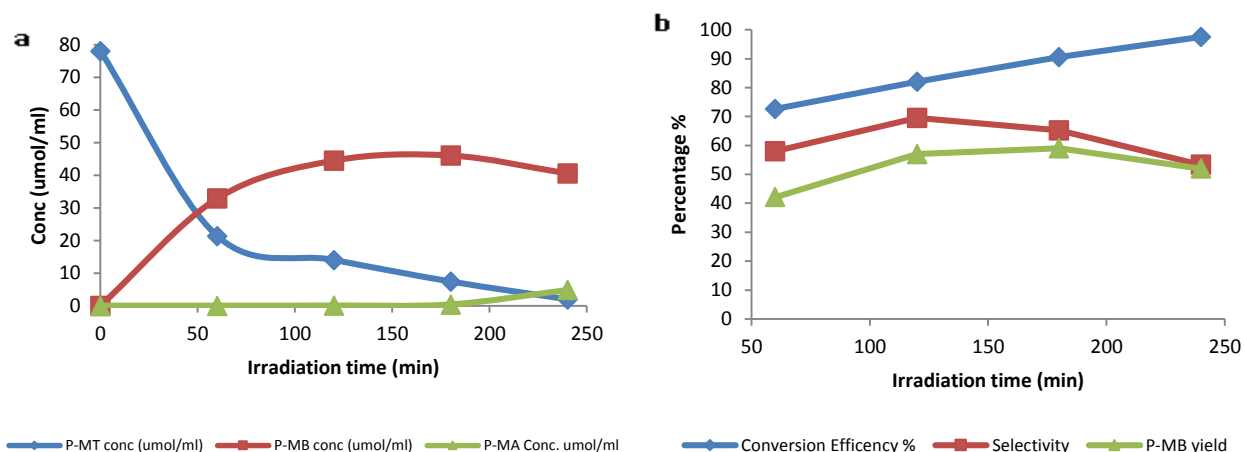


Fig. 5. Time online photocatalytic oxidation reaction of p-methoxy toluene (p-MT) under UV irradiation, conversion efficiency, selectivity and yield over TiO₂ p25 nanoparticles (a and b) and TiO₂/graphene composite (c and d)

Table. 1. TiO₂ p25 nanoparticles in comparison to TiO₂/graphene composite.

	BET specific surface area (m ² /g)	Mean Pore diameter [nm]	Total pore volume [cm ³ /g]	Conversion Efficiency (4 hrs) [%]	Maximum Yield [%]	Maximum Selectivity [%]	Rate [min ⁻¹] / R ²
TiO ₂ p25	52.95	15.92	0.2108	98	69	57	0.014/0.961
TiO ₂ /Graphene	55.62	28.60	0.3978	99	76	65	0.021/0.890

Acknowledgements

The first author is very grateful for Ministry of Higher Education (MOHE) for giving him a scholarship to study his Ph.D at Egypt-Japan University of Science and Technology (E-JUST).

References

- Fujishima, A., & Honda, K. (1972). Electrochemical Photolysis Of Water At A Semiconductor Electrode. *Nature*, 238, 37.
- Geim, a K. (2009). Graphene: Status And Prospects. *Science (New York, N.Y.)*, 324(5934), 1530–1534. DOI: <http://doi.org/10.1126/science.1158877>
- Geim, a K., Novoselov, K. S., Geim A. K., & Novoselov, K. S. (2007). The Rise Of Graphene. *Nat. Mater.*, 183–191. DOI: <http://doi.org/http://dx.doi.org/10.1038/nmat1849>
- Hoffmann, M. R., Martin, S. T., Choi, W., & Bahnemannt, D. W. (1995). Environmental Applications of Semiconductor Photocatalysis. *Chemical Reviews*, 95(1), 69–96. DOI: <http://doi.org/10.1021/cr00033a004>
- Kenneth, S., Sing, W., Douglas, H., Everett, R. A., Haul, W., Moscou, L., Pierotti, R. A., Rouquerol, J., & T. S. (1985). Reporting Physisorption Data for Gas/Solid Systems. *Pure Appl. Chem.*, 57, 603–619.
- Ksibi, M., Rossignol, S., Tatibouët, J. M., & Trapalis, C. (2008). Synthesis And Solid Characterization Of Nitrogen And Sulfur-Doped Tio2 Photocatalysts Active Under Near Visible Light. *Materials Letters*, 62(26), 4204–4206. DOI: <http://doi.org/10.1016/j.matlet.2008.06.026>
- Kudo, A., & Miseki, Y. (2009). Heterogeneous Photocatalyst Materials For Water Splitting. *Chemical Society Reviews*, 38(1), 253–278. DOI: <http://doi.org/10.1039/b800489g>

- Lee, S., Park, J., & Joo, H. (2006). Visible Light-Sensitized Photocatalyst Immobilized On Beads By CVD In A Fluidizing Bed. *Solar Energy Materials and Solar Cells*, 90(13), 1905–1914. DOI: <http://doi.org/10.1016/j.solmat.2005.11.009>
- Mallat, T., & Baiker, A. (2004). Oxidation of Alcohols with Molecular Oxygen on Solid Catalysts. *Chem. Rev.*, (104), 3037–3058.
- Marcano, D. C., Kosynkin, D. V, Berlin, J. M., Sinitskii, A., Sun, Z., Slesarev, A., & Tour, J. M. (2010). Improved Synthesis of Graphene Oxide. *ACS Nano*, 4(8), 4806–4814.
- Mueller, J. A., Goller, C. P., & Sigman, M. S. (2004). Elucidating the Significance of -Hydride Elimination and the Dynamic Role of Acid / Base Chemistry in a Palladium-Catalyzed Aerobic Oxidation of Alcohols. 9724–9734.
- Palmisano, G., Augugliaro, V., Pagliaro, M., & Palmisano, L. (2007). Photocatalysis: A Promising Route For 21st Century Organic Chemistry. *Chemical Communications (Cambridge, England)*, (33), 3425–37. DOI: <http://doi.org/10.1039/b700395c>
- Palmisano, G., García-López, E., Marci, G., Loddo, V., Yurdakal, S., Augugliaro, V., & Palmisano, L. (2010). Advances In Selective Conversions By Heterogeneous Photocatalysis. *Chemical Communications (Cambridge, England)*, 46(38), 7074–89. DOI: <http://doi.org/10.1039/c0cc02087g>
- Pan, X., Zhao, Y., Liu, S., Korzeniewski, C. L., Wang, S., & Fan, Z. (2012). Comparing Graphene-TiO₂ Nanowire and Graphene-TiO₂ Nanoparticle Composite Photocatalysts. *ACS Appl. Mater. Interfaces*, 4, 3944–3950.
- Park, J. H., Kim, S., & Bard, A. J. (2006). Novel Carbon-Doped TiO₂ Nanotube Arrays With High Aspect Ratios For Efficient Solar Water Splitting. *Nano Letters*, 6(1), 24–28. DOI: <http://doi.org/10.1021/nl051807y>
- The-effects-of-sintering-on-the-photocatalytic-activity-of-N-Doped-TiO-2-nanoparticles_2008_Chemistry-of-Materials. (n.d.).
- Yang, M., Zhang, N., & Xu, Y. (2013). Synthesis of Fullerene – , Carbon Nanotube – , and Graphene – TiO₂ Nanocomposite Photocatalysts for Selective Oxidation : A Comparative Study.
- Zhang, M., Wang, Q., Chen, C., Zang, L., Ma, W., & Zhao, J. (2009). Oxygen Atom Transfer in the Photocatalytic Oxidation of Alcohols by TiO₂ : Oxygen Isotope Studies. *Angewandte Chemie International Edition*, 48(33), 6081–6084. DOI: <http://doi.org/10.1002/anie.200900322>
- Zhang, N., Zhang, Y., Pan, X., Fu, X., Liu, S., & Xu, Y. (2011). Assembly of CdS Nanoparticles on the Two-Dimensional Graphene Scaffold as Visible-Light-Driven Photocatalyst for Selective Organic Transformation under Ambient Conditions. 23501–23511.